Cell Metabolism
Short Article

Iron Regulatory Proteins Secure Mitochondrial Iron Sufficiency and Function

Bruno Galy,[1] Dunja Ferring-Appel,[1] Sven W. Sauer,[2] Sylvia Kaden,[3] Saïd Lyoumi,[4,5] Herve Puy,[4,5] Stefan Kölker,[2] Hermann-Josef Gröne,[3] and Matthias W. Hentze[1,*]
[1]European Molecular Biology Laboratory, Meyerhofstrasse 1, 69117 Heidelberg, Germany
[2]Department of General Pediatrics, Division of Inherited Metabolic Disease, University Children's Hospital Heidelberg, Im Neuenheimer Feld 430, 69120 Heidelberg, Germany
[3]Deutsches Krebsforschungszentrum Heidelberg, Im Neuenheimer Feld 280, 69120 Heidelberg, Germany
[4]Centre Français des Porphyries, Hôpital Louis Mourier, 178 rue des Renouillers, 92701 Colombes CEDEX, France
[5]INSERM Unité 773, Centre de Recherches Biomédicales Bichat-Beaujon, Université de Versailles Saint-Quentin en Yvelines, 75018 Paris, France
*Correspondence: hentze@embl.de
DOI 10.1016/j.cmet.2010.06.007

SUMMARY

Mitochondria supply cells with ATP, heme, and iron sulfur clusters (ISC), and mitochondrial energy metabolism involves both heme- and ISC-dependent enzymes. Here, we show that mitochondrial iron supply and function require iron regulatory proteins (IRP), cytosolic RNA-binding proteins that control mRNA translation and stability. Mice lacking both IRP1 and IRP2 in their hepatocytes suffer from mitochondrial iron deficiency and dysfunction associated with alterations of the ISC and heme biosynthetic pathways, leading to liver failure and death. These results uncover a major role of the IRPs in cell biology: to ensure adequate iron supply to the mitochondrion for proper function of this critical organelle.

INTRODUCTION

Maintenance of cellular and organismal iron balance requires adequate iron uptake and prevention of toxic iron excess (Andrews, 2008). At the systemic level, the hepatic "iron hormone" hepcidin (Hamp) has emerged as the key regulator of blood iron levels (Nemeth and Ganz, 2006). At the cellular level, in vitro and cell culture studies have shown that IRP-1 and –2 enact posttranscriptional regulation of critical iron metabolism genes via their interaction with *cis*-regulatory iron-responsive elements (IRE) present on target mRNAs, especially for the transferrin receptor, the iron storage protein ferritin, and the iron exporter ferroportin (FPN)/SLC40A1 (Muckenthaler et al., 2008; Wallander et al., 2006). However, the overarching biological function(s) of the IRP/IRE regulatory network in cellular physiology remain(s) to be defined.

Mouse models of IRP deficiency have recently become available to explore the in vivo functions of the IRP/IRE system (Galy et al., 2005a; LaVaute et al., 2001; Meyron-Holtz et al., 2004). Whereas mice with systemic deficiency for either IRP are viable and fertile (Galy et al., 2005b), doubly deficient animals die during early embryogenesis (Galy et al., 2008; Smith et al., 2006), showing that the IRP/IRE system is essential and that the two IRPs are functionally redundant. The lethality of mice with compound IRP deficiency combined with strong functional redundancy between the two proteins poses a challenge to elucidating the IRPs' cell biological function(s).

To bypass this problem, we simultaneously ablated IRP1 and IRP2 in a tissue-specific manner using Cre/Lox technology (Garcia and Mills, 2002). We inactivated the *Aco1* and *Ireb2* genes in hepatocytes, the major storage depot for excess iron in the body and the source of the systemic iron hormone hepcidin (Graham et al., 2007). Our study shows that the IRP/IRE system plays a critical role for mitochondrial iron management and function and is essential for liver physiology and organismal survival.

RESULTS AND DISCUSSION

Hepatocytic IRP Deficiency Causes Lethal Liver Failure

Mice homozygous for floxed *Aco1* and *Ireb2* alleles ($Aco1^{flox/flox}$, $Ireb2^{flox/flox}$) (Galy et al., 2008) were bred to a transgenic line (*Alfp-Cre*) expressing Cre recombinase under the control of the *Albumin/α−fetoprotein* regulatory elements selectively in hepatocytes, starting at E9.5–E10.5 (Kellendonk et al., 2000). $Aco1^{flox/flox}$,$Ireb2^{flox/flox}$,*Alfp-Cre* animals ($Irp^{Alfp\text{-}Cre(+)}$) are born at nearly Mendelian ratios (see Table S1 available online) and are macroscopically indistinguishable from control littermates lacking the *Alfp-Cre* transgene ($Irp^{Alfp\text{-}Cre(-)}$) at birth; however, all $Irp^{Alfp\text{-}Cre(+)}$ mice die between 8 and 12 days postpartum (p.p.) (Figure 1A and Table S1). Southern blotting ascertained liver-specific Cre recombination of the floxed *Irp* alleles (Figure S1). At 8 days p.p., $Irp^{Alfp\text{-}Cre(+)}$ mice appear wasted (Figure 1B), with a 25% reduction of body weight (Figure 1C). Although hepatic *Hepcidin* expression is downregulated to ~30% of control levels (Figure S2), hematological and blood chemistry parameters reveal no sign of systemic iron abnormalities (Table 1); *Hepcidin* downregulation in the context of unchanged transferrin saturation is unexpected and could plausibly be due to cellular damage and/or intracellular iron depletion (see below and Figure S2). Serum ferritin levels are elevated, possibly due to secretion from IRP-deficient hepatocytes that overexpress ferritin (Figure S3) and/or release into the bloodstream as a consequence of cell damage (see below).

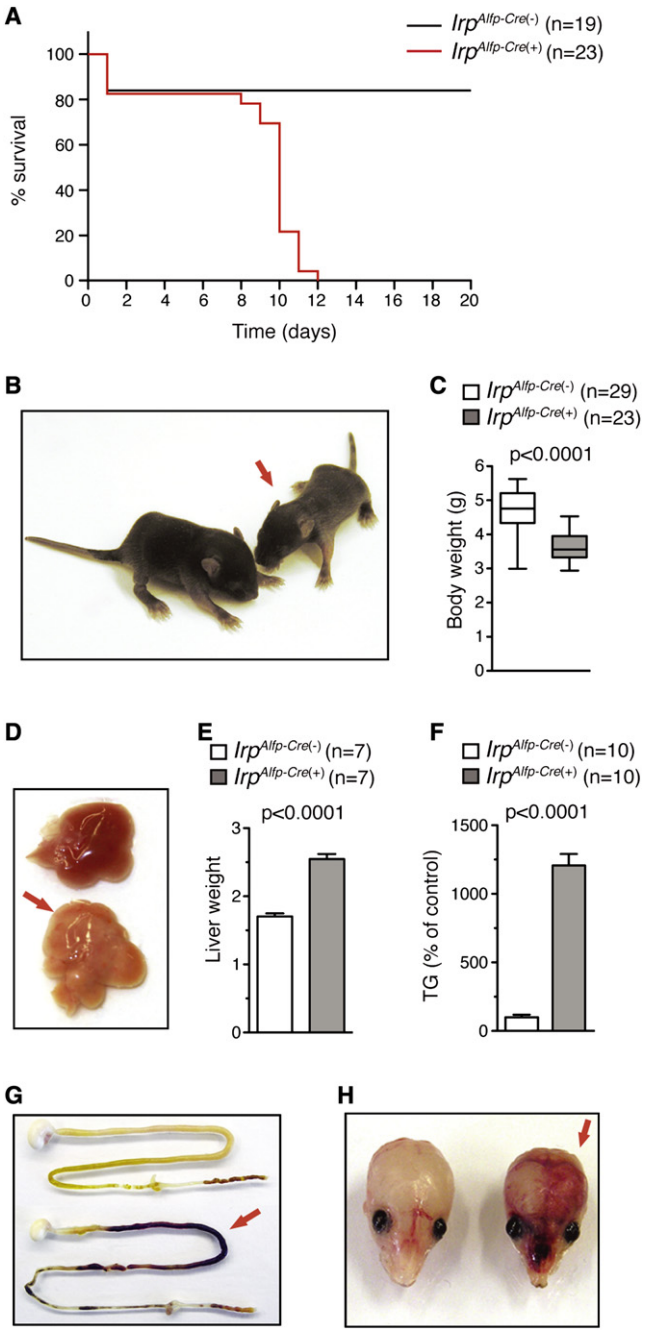

Figure 1. Liver Failure and Early Death of Mice with Complete Hepatocytic IRP Deficiency

(A) Kaplan-Meyer survival curves showing preweaning lethality of $Irp^{Alfp\text{-}Cre(+)}$ mice (red curve) compared to $Irp^{Alfp\text{-}Cre(-)}$ littermates (black curve).

(B) Mice with hepatocytic IRP deficiency (red arrow) at 8 days of age; an $Irp^{Alfp\text{-}Cre(-)}$ control littermate lacking Cre recombinase expression is also shown.

(C) Body weight, box-plot representation with minimal to maximal values.

(D) Enlargement and fatty appearance of the liver in 8-day-old $Irp^{Alfp\text{-}Cre(+)}$ animals (red arrow) compared to control.

(E and F) (E) Liver weight (square root of 100 × [liver weight/body weight]) and (F) hepatic triglyceride (TG) content. Data are presented as means ± SEM. The sample size (n) is indicated; p values were determined by Student's t test.

(G and H) Signs of internal bleeding in the intestine (G) and the brain (H) of $Irp^{Alfp\text{-}Cre(+)}$ mice (red arrow); a control sample is shown for comparison.

See also Figure S1 and Table S1.

Table 1. Hematological and Blood Chemistry Parameters of Mice Lacking Both IRP1 and IRP2 in Hepatocytes

		$Irp^{Alfp\text{-}Cre(-)}$	n	$Irp^{Alfp\text{-}Cre(+)}$	n	p
Blood Chemistry						
Plasma Fe	(μmol/l)	41.8 ± 4.8	16	46.3 ± 11.1	12	0.717
UIBC	(μmol/l)	116.0 ± 1.4	16	116.9 ± 1.5	12	0.664
TIBC	(μmol/l)	157.8 ± 4.6	16	163.2 ± 10.9	12	0.658
Tf sat.	(%)	25.7 ± 2.1	16	25.8 ± 3.6	12	0.968
Ferritin	(ng/ml)	86 ± 7	12	4045 ± 448	9	<0.0001
Albumin	(g/l)	12.0 ± 0.6	12	10.8 ± 0.4	9	0.132
Total protein	(g/l)	31.3 ± 0.5	12	27.0 ± 0.3	9	<0.0001
Total bilirubin	(μmol/l)	2.6 ± 0.1	10	45.7 ± 4.9	9	<0.0001
Conj. bilirubin	(μmol/l)	0.6 ± 0.2	10	21.0 ± 2.6	9	<0.0001
AP	(U/l)	815 ± 43	12	1682 ± 178	9	<0.01
ALT	(U/l)	16 ± 1	12	32 ± 4	9	<0.01
AST	(U/l)	117 ± 9	12	257 ± 11	9	<0.0001
Hydroxybutyrate	(mmol/l)	1.06 ± 0.07	12	0.96 ± 0.26	9	0.262
Hematology						
WBC count	(10^9/l)	7.93 ± 0.86	25	7.75 ± 0.74	18	0.698
RBC count	(10^{12}/l)	4.54 ± 0.09	25	4.82 ± 0.13	18	0.079
MCV	(fl)	62.3 ± 0.7	25	68.1 ± 2.5	18	0.765
RDW	(%)	16.4 ± 0.3	25	16.7 ± 0.3	18	0.448
Hemoglobin	(g/l)	108 ± 3	25	117 ± 4	18	0.075
Hematocrit	(%)	30.6 ± 0.7	25	32.8 ± 0.8	18	0.056
MCH	(pg)	23.8 ± 0.6	25	24.8 ± 1.5	18	0.549
MCHC	(g/l)	353 ± 8	25	362 ± 19	18	0.658
Platelet count	(10^9/l)	177 ± 48	25	273 ± 42	18	0.142
MPV	(fl)	6.44 ± 0.10	25	6.31 ± 0.11	18	0.411

Hematological and blood chemistry parameters of $Irp^{Alfp\text{-}Cre(+)}$ versus $Irp^{Alfp\text{-}Cre(-)}$ mice were determined at 8 days of age. Data are given as averages ± SEM. The sample size (n) is indicated. p represents the value of a Student's t test (unpaired, two-tailed). UIBC, unsaturated-iron binding capacity; TIBC, total iron-binding capacity; Tf sat., transferrin saturation; Conj. bilirubin, conjugated bilirubin; AP, alkaline phosphatase; ALT, alanine aminotransferase; AST, aspartate aminotransferase; WBC, white blood cell; RBC, red blood cell; MCV, mean corpuscular volume; RDW, red blood cell distribution width; MCH, mean corpuscular hemoglobin; MCHC, mean corpuscular hemoglobin concentration; MPV, mean platelet volume. See also Figure S2 and Table S2.

$Irp^{Alfp\text{-}Cre(+)}$ mice display hepatic steatosis (Figure 1D), with increased liver weight (Figure 1E) and hepatic triglyceride (TG) levels (Figure 1F); the steatosis is further evident from the presence of multiple lipid droplets on periodic acid Schiff stains (Figures 2A to 2D) and on electron micrographs (Figures 2G and 2H). Normal levels of plasma hydroxybutyrate (Table 1) and acylcarnitines (Table S2) rule out impaired β-oxidation as a possible cause of hepatic lipid loading. Normal liver weight and TG content in *Alfp-Cre* mice (Figure S1) show that the hepatic steatosis in $Irp^{Alfp\text{-}Cre(+)}$ animals is not an artifact due to the *Alfp-Cre* transgene per se (Schmidt-Supprian and Rajewsky, 2007).

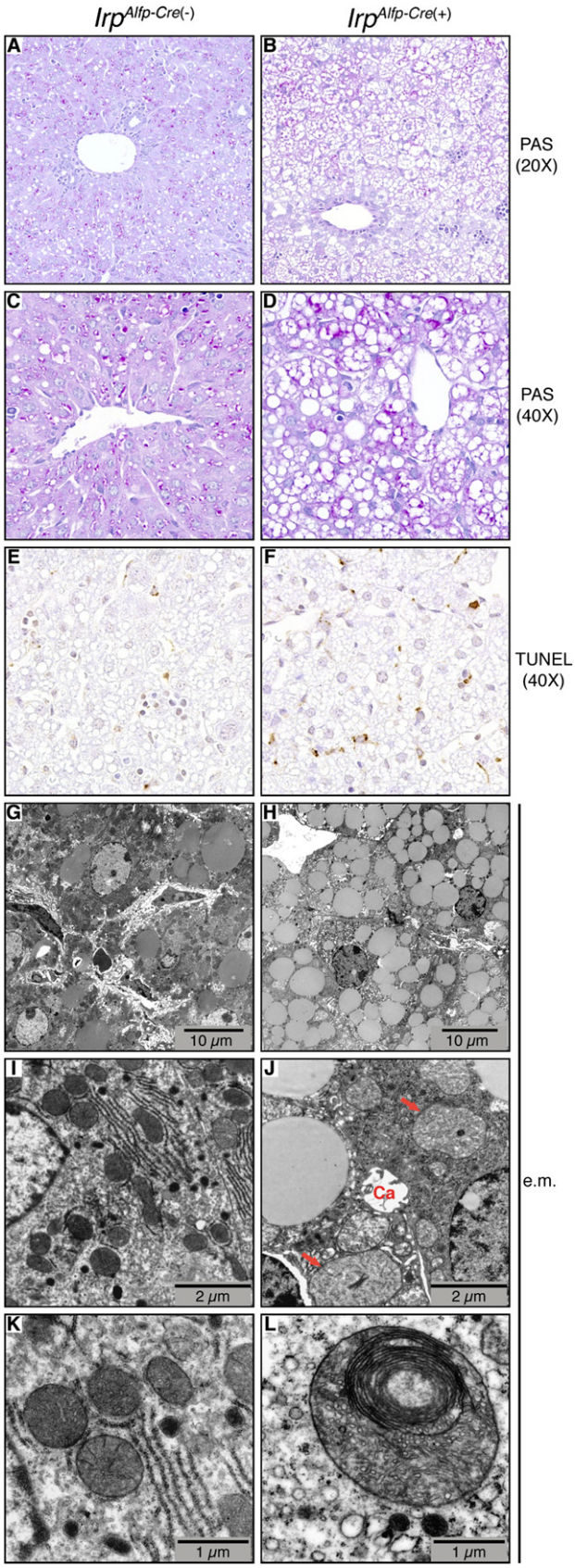

Figure 2. Histological and Ultrastructural Abnormalities in the Liver of Mice Lacking Hepatocytic IRP Expression

Histological (A–F) and ultrastructural (G–L) analyses of the liver of 8- to 9-day-old $Irp^{Alfp\text{-}Cre(+)}$ mice (B, D, F, H, J, and L) compared to control littermates (A, C, E, G, I, and K).

(A–D) Periodic acid Schiff (PAS) staining reveals numerous vacuoles in the liver of $Irp^{Alfp\text{-}Cre(+)}$ mice, typical of steatosis. Original magnifications: (A and B) 20×, (C and D), 40×.

(E and F) TUNEL staining showing increased cell death (dark brown cells, counterstain: hemalaun) in IRP-deficient livers. Original magnification: 40×.

(G and H) Electron micrographs showing abundant lipid droplets in the liver of mutant mice.

(I–L) At high magnification, mitochondria in IRP-deficient hepatocytes (J) appear large and pale with poor cristae structure (red arrows) as compared to control (I). They occasionally contain myelin-like structures that are not present in control cells. An intact canaliculus (indicated Ca) is shown in (J).

Though we observed no sign of fibrosis nor inflammatory cell infiltrates (Figures 2A and 2B), TUNEL staining revealed increased cell death in IRP-deficient livers (Figure 2F). Several observations point to compromised liver function/integrity: (1) a tendency for decreased albumin concentration and a significant reduction in plasma protein levels (Table 1), (2) signs of internal bleeding in the intestine and/or the brain of some moribund animals (Figures 1G and 1H) plausibly due to inadequate hemostasis, and (3) increased serum alanine aminotransferase and aspartate aminotransferase (Table 1). Furthermore, increased plasma alkaline phosphatase and conjugated bilirubin indicate posthepatic cholestasis, although the bile canaliculi themselves appear ultrastructurally normal in shape and number (Figure 2J). Collectively, these data show that the early lethality of mice with hepatocytic IRP deficiency is unrelated to *Hepcidin* dysregulation or systemic abnormalities of iron metabolism but likely results from hepatic failure. Hepatocytic IRP expression thus appears to be indispensable for liver function and organismal survival.

Mitochondriopathy in IRP-Null Livers

Hepatic steatosis could have multiple causes affecting lipid synthesis, catabolism, and/or trafficking; mitochondrial dysfunction has emerged as a key feature of the pathogenesis of fatty liver diseases (Mantena et al., 2008). Consistent with this, mitochondriopathy represents the most prominent ultrastructural abnormality associated with persistent lipid accumulation in IRP-deficient hepatocytes. Mitochondria are swollen, imposing with a hypodense matrix and poor cristae structure (Figure 2J), occasionally showing myelin-like figures (Figure 2L); the other cellular organelles and structures appear normal.

To explore the cause(s) of the mitochondrial abnormalities in IRP deficiency, we assayed enzymatic activities of the electron transport chain (ETC) and the tricarboxylic acid (TCA) cycle. The activity of complexes I, II, and III of the ETC (Figure 3A) is markedly reduced, whereas complex IV is unaltered and ATP synthase activity slightly increased. The ETC in the heart is intact (Figure 3A), showing that the impairment of complexes I–III is liver specific and not systemic. Likewise, analysis of TCA cycle enzymes (Figure 3B) reveals a dramatic drop in the activity of the 2-oxoglutarate dehydrogenase complex and significantly altered citrate synthase, pyruvate dehydrogenase complex,

fumarase, and malate dehydrogenase activities; the 70% reduction of total aconitase activity (mitochondrial plus cytosolic = IRP1) reflects the lack of IRP1 and, likely, impaired function of the mitochondrial isoform. These data show that IRP deficiency in hepatocytes affects two of the central metabolic functions of mitochondria, the ETC and the TCA cycle.

Mitochondrial Iron Deficiency and Compromised Heme and ISC Biogenesis

What links the IRP/IRE system to mitochondrial function? Both iron excess and deficiency may cause mitochondrial impairment (Atamna et al., 2002). We therefore assayed total nonheme iron levels in whole-liver extracts and found an ~50% reduction in $Irp^{Alfp\text{-}Cre(+)}$ mice (Figure 3C). To better understand the cause(s) for decreased hepatic iron content, we analyzed the expression of iron-related genes, focusing on IRP targets. As expected, IRP ablation strongly enhances the posttranscriptional expression of both the ferritin H and L chains and leads to a marked decrease in the protein and mRNA levels of transferrin receptor 1 (TFRC) (Figures S3A and S3B). FPN is also posttranscriptionally increased, whereas the IRE-containing SLC11A2 (solute carrier family 11 member 2)/DMT1 mRNA variant is downregulated. Although not a direct IRP target, the expression of the mRNA encoding the putative nontransferrin-bound iron uptake molecule SLC39A14 (solute carrier family 39 member 14)/ZIP14 (Liuzzi et al., 2006) is also reduced (Figure S3C). The expression of IRE-containing genes not directly involved in the control of hepatocytic iron fluxes was analyzed as well (data presented in Figure S3). Upregulation of the iron exporter FPN combined with downregulation of iron acquisition molecules (TFRC, SLC11A2, SLC39A14) can explain the reduction of the total hepatic iron content in $Irp^{Alfp\text{-}Cre(+)}$ mice. Because mitochondrial iron overload can coexist with cytosolic iron depletion and vice versa (Paradkar et al., 2009; Shaw et al., 2006; Tong and Rouault, 2006) and because mitochondria appear to contribute a relatively small fraction of total liver iron at a given time, at least in adult rats (Swick et al., 1982), we also determined iron levels in isolated mitochondria (Figure S4A) and found an ~50% reduction in IRP-null livers (Figure 3D). The IRP/IRE system thus controls iron management proteins, which is critical for securing mitochondrial iron supplies. Of note, the SLC25A28 (a.k.a. mitoferrin 2) mitochondrial iron uptake molecule is severely downregulated in IRP deficiency, whereas expression levels of its SLC25A37 (a.k.a. mitoferrin 1) paralog remain unchanged (Figures S4A and S4B); this alteration most probably represents an indirect effect of IRP deficiency, as SLC25A28 mRNA bears no recognizable IRE-like motif. Although the importance of SLC25A28 for mitochondrial iron uptake in mouse hepatocytes has not yet been formally assessed, SLC25A28 downregulation in $Irp^{Alfp\text{-}Cre(+)}$ animals would be expected to contribute to the observed mitochondrial iron deficiency.

We next asked how mitochondrial iron deficiency affects cellular physiology. Mitochondria convert iron into essential bioactive prosthetic groups, i.e., heme and iron sulfur clusters (ISC) that are utilized both by the mitochondrion itself and throughout the cell (Levi and Rovida, 2009; Sheftel and Lill, 2009). Complexes I–III (ETC) and ACO2 (TCA cycle) are dependent on ISC; impairment of their activity in IRP-deficient livers (Figures 3A and 3B) could therefore be a sign of altered ISC metabolism. Supporting this notion, the activities of the extramitochondrial ISC protein xanthine dehydrogenase and the mitochondrial ferrochelatase are also reduced by 75% and 90%, respectively, associated with only a minor decrease (~25%) in the steady-state levels of the corresponding proteins (Figures 3E and 3F). We also observe decreased expression of mature phosphoribosyl pyrophosphate amidotransferase (PPAT) (Figure S4C), a cytosolic protein whose processing requires the assimilation of an ISC. These data show that IRP deficiency impairs both mitochondrial and extramitochondrial ISC proteins, probably as a consequence of impaired ISC biogenesis in mitochondria.

Ferrochelatase catalyzes the insertion of iron into protoporphyrin to form heme; hence, decreased ferrochelatase activity (see above) combined with mitochondrial iron deficiency should both negatively affect heme biosynthesis (Ajioka et al., 2006). Indeed, heme levels are reduced in the liver of $Irp^{Alfp\text{-}Cre(+)}$ mice, with the expected concomitant protoporphyrin accumulation (Figure 3G); the accumulated protoporphyrin is essentially free, with no detectable Zn-protoporphyrin. The ETC complex IV is a hemoprotein; in spite of decreased heme levels, its activity is not altered in IRP-null livers (Figure 3A). Similarly, the activity of catalase, an extramitochondrial hemoprotein, is preserved (Figure 3H). Although nonhepatocytic liver cells could mitigate the effect of hepatocytic IRP deficiency in whole-tissue measurements, these data are consistent with the reported preservation of the heme regulatory pool in $Fech^{m1Pas}$ mice expressing less than 5% of normal liver ferrochelatase activity (Davies et al., 2005); it appears that ferrochelatase is in significant excess in liver cells, as opposed to erythroblasts in which the enzyme is limiting (Puy et al., 2010). Although we cannot rule out that other heme-dependent molecules could be affected, the data suggest that ISC proteins are more sensitive to IRP deficiency than hemoproteins and might thus represent the "Achilles heel." Collectively, these data show that IRP deficiency causes mitochondrial dysfunction with mitochondrial iron deficiency and ensuing alterations of the ISC and heme biosynthetic pathways (Figure 3I).

The marked mitochondrial dysfunction in $Irp^{Alfp\text{-}Cre(+)}$ mice with only a 2-fold reduction of total liver iron levels contrasts with previous reports that also showed mitochondrial enlargement in the liver of rats subjected to dietary iron restriction (Dallman and Goodman, 1970) but largely preserved mitochondrial function (e.g., Dallman, 1986). Many studies have shown remarkable resistance of liver mitochondria to iron deficiency unless rigid regimen made animals severely anemic with a strong depletion of the hepatic iron stores (e.g., Masini et al., 1994). As our iron measurements include all liver cells, the contribution of nonhepatocytes may partially mask a more severe reduction of hepatocytic iron levels. More importantly, the physiological response to iron deficiency is IRP activation and ferritin downregulation (see, e.g., Chen et al., 1997). In IRP-deficient hepatocytes, ferritin expression is completely derepressed in spite of iron deficiency. The failure of IRP-null hepatocytes to decrease iron sequestration in ferritin in the context of low iron levels would therefore be predicted to further limit cellular iron bioavailability, thereby creating a state of functional iron deficiency more drastic than indicated by measurements of total liver iron. If true, co-ablation of ferritin together with IRPs would be predicted

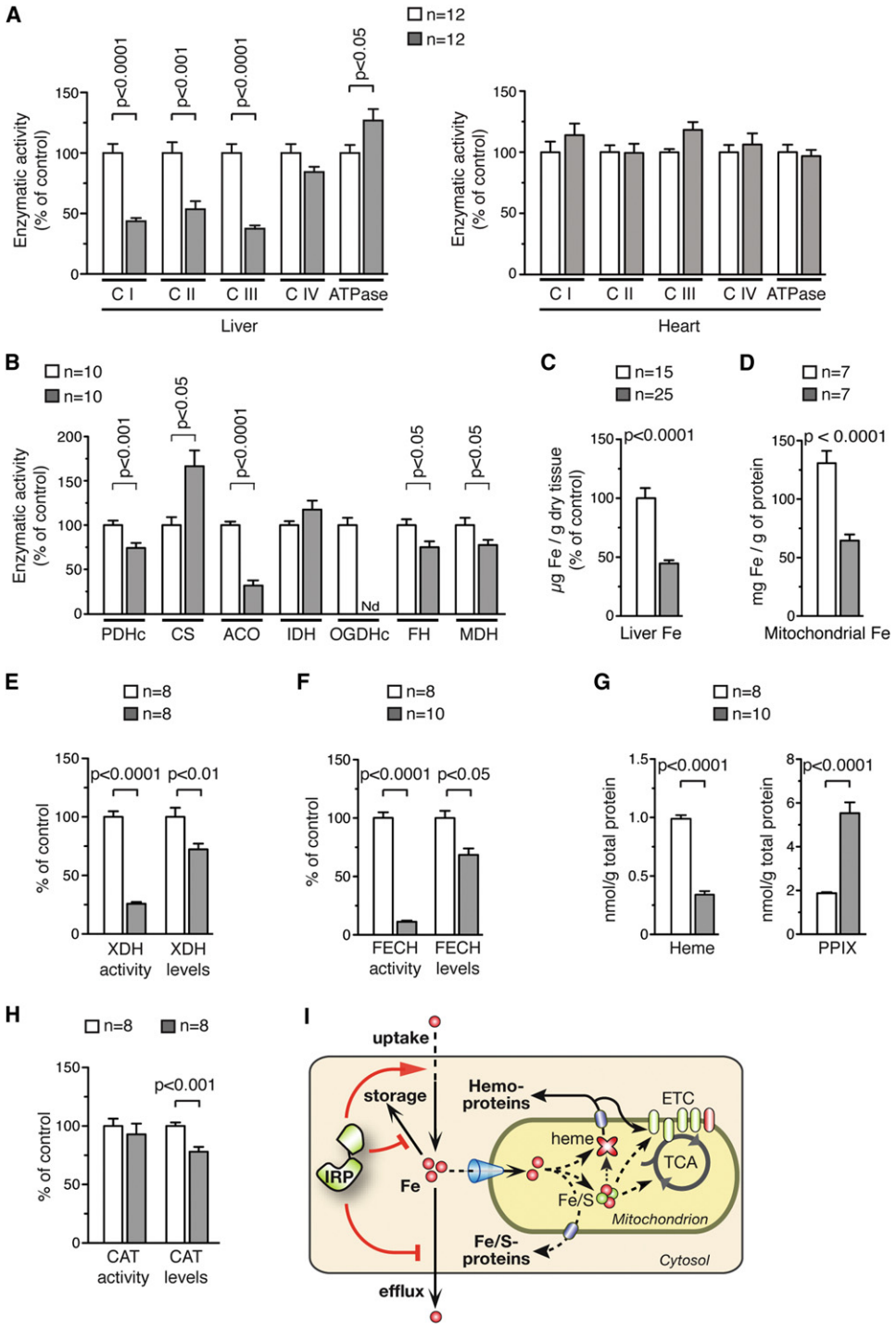

Figure 3. Mitochondrial Iron Deficiency and Function Associated with Altered Iron Sulfur Cluster and Heme Metabolism in IRP-Deficient Livers

(A–H) Multiple biochemical parameters were assayed in liver samples of 8-day-old *Irp*$^{Alfp\text{-}Cre(+)}$ mice (gray bars) versus control *Irp*$^{Alfp\text{-}Cre(-)}$ littermates (open bars): enzymatic activities of (A) the electron transport chain (left, liver; right, heart) and (B) the TCA cycle; nonheme iron levels in (C) the entire liver or (D) isolated mitochondria; activity and expression levels of (E) xanthine dehydrogenase (XDH), (F) ferrochelatase (FECH), and (H) catalase (CAT); and heme and free protoporphyrin (PPIX) levels (G). Data are presented as means ± SEM. The sample size (n) is indicated. p values were determined by Student's t test.

CI (complex I), NADH-ubiquinone oxidoreductase; CII (complex II), succinate dehydrogenase; CIII (complex III), ubiquinol-cytochrome c oxidoreductase; CIV (complex IV), cytochrome c oxidase; PDHc, pyruvate dehydrogenase complex; CS, citrate synthase; ACO, aconitase 2; IDH, isocitrate dehydrogenase; OGDHc, oxaloglutarate dehydrogenase complex; MDH, malate dehydrogenase; FH, fumarate hydratase; Nd, not detectable.

to (partially) alleviate the mitochondrial iron deficiency of $Irp^{Alfp\text{-}Cre(+)}$ mice.

Recent studies of human genetic diseases and animal models have highlighted the importance of mitochondrial iron metabolism (Levi and Rovida, 2009; Sheftel and Lill, 2009). This is exemplified by the mitochondrial iron loading in pathologies associated with abnormal ISC metabolism such as Friedreich's ataxia, the myopathy due to ISCU deficiency, or sideroblastic anemias due to defects in e.g., the *Grx5*, *Slc25A38*, or *Abcb7* genes (Guernsey et al., 2009; Levi and Rovida, 2009; Rouault and Tong, 2008; Sheftel and Lill, 2009). It has been hypothesized that impaired ISC biogenesis causes missignaling of the mitochondrial iron status, causing increased mitochondrial iron uptake and/or decreased efflux (Huang et al., 2009, Tong and Rouault, 2006).

IRP-deficient hepatocytes display decreased cellular iron uptake (TFRC, SLC11A2, and SLC39A14) combined with increased sequestration within ferritin and efflux via FPN. These alterations decrease iron availability, limiting mitochondrial iron supplies. In addition, IRP deficiency leads to reduced SLC25A28 expression, which may further limit mitochondrial iron uptake as observed in mitoferrin-deficient cells (Paradkar et al., 2009; Shaw et al., 2006), resulting in impaired heme and ISC metabolism and mitochondrial dysfunction (Figure 3I) with widespread alterations of iron-containing proteins throughout the cell. Furthermore, the lack of IRPs precludes the normal response to impaired ISC biogenesis, which is IRP-mediated adjustment of cellular iron uptake, storage, and export (Tong and Rouault, 2006). In the absence of IRPs, mitochondria fail to combat iron deficiency. The same mechanism could explain the mitochondriopathy recently observed in enterocytes lacking IRP expression (Galy et al., 2008; Smith et al., 2006), and we propose that it represents a general function of IRPs in cell biology.

By contrast, impaired ISC biogenesis with abnormally high IRP activity appears to maintain cellular iron levels constitutively high, triggering mitochondrial iron (over)loading. Whether and how mitochondria can protect themselves against iron overload remains to be elucidated. This work shows that IRP function protects mitochondria against detrimental iron deficiency, a vital mechanism that, at least in cases of, e.g., Friedreich's ataxia, appears to override the hypothetical protective measures against mitochondrial iron overload.

EXPERIMENTAL PROCEDURES

Mice

For all studies of $Irp^{Alfp\text{-}Cre(+)}$ mice, controls consisted of $Irp^{Alfp\text{-}Cre(-)}$ littermates. Mice were backcrossed to C57BL6 mice for at least 10 generations. Whereas 4-day-old $Irp^{Alfp\text{-}Cre(+)}$ mice displayed normal mitochondrial ultrastructure and no histological sign of apoptosis, mitochondriopathy appeared in 6-day-old animals and was fully penetrant at 8 days of age (data not shown). Hence, all assays were carried out using 8-day-old animals. Mice were kept under a constant light/dark cycle on a standard diet. They were sacrificed by CO_2 inhalation, and heparinized blood was collected by cardiac puncture. Animal handling was in accordance with approved EMBL guidelines.

Hematology and Blood Chemistry

Hematological and plasma iron parameters were determined as described previously (Galy et al., 2008). Plasma alanine aminotransferase and aspartate aminotransferase levels, respectively, were determined using the ALT/TGP and AST/TGO kits (Biolabo, Maizy, France). All other plasma chemistry parameters were determined by the Claude Bernard Institute Chemistry Laboratory (Paris, France) using an Olympus 400 analyzer.

Measurement of Hepatic Triglyceride Levels

Lipids were extracted from liver homogenates with chloroform:methanol (2:1) and, after dessication, resuspended in isopropanol + 10% Triton X-100 as described (Yang et al., 2009). TG were assayed spectrophotometrically using the TG/GPO kit (Biolabo). TG levels were standardized to protein levels in the initial homogenate as determined using the D_C protein assay (BioRad, München, Germany).

Immunoblotting

Tissues were pulverized in liquid nitrogen and homogenized in RIPA buffer complemented with inhibitors of proteases (Galy et al., 2005b) and of phosphatases (phosphatase inhibitor cocktail 2, Sigma-Aldrich, Taufkirchen, Germany). Lysates were incubated for 30 min on ice and centrifuged at 14,500 × g for 15 min at 4°C. The supernatant was stored at −80°C until use. For immunodetection of EPAS1 and LAMIN-A, the pellet was resuspended in 20 mM HEPES (pH 7.4), 400 mM NaCl, and 1 mM EDTA + protease inhibitors and incubated for 30 min on ice. After sonication in a Bioruptor (Diagenode, Liège, Belgium), debris was pelleted by centrifugation at 14,500 × g for 20 min at 4°C. Immunoblotting was performed using the primary antibodies listed in Supplemental Experimental Procedures, together with HRP-conjugated secondary antibodies. For quantification of CAT, FECH, PPAT, and XDH expression, we used fluorescently labeled secondary antibodies together with an Odyssey infrared imaging system (LI-COR Biosciences GmbH, Homburg, Germany); CAT, FECH, PPAT, and XDH levels were calibrated to β-ACTIN expression.

Enzymatic Assays

Catalase

Liver tissues were homogenized in 50 mM KPO_4 (pH 7.0) and 1 mM EDTA, and debris was pelleted by centrifugation at 10,000 × g for 15 min at 4°C. Enzyme activity was measured using the catalase assay kit from Cayman (Cayman Europe, Tallin, Estonia) and standardized to total protein concentration.

Xanthine Dehydrogenase

Tissues were homogenized in 100 mM KPO_4 (pH 7.5), 2.5 mM EDTA, and 5 mM DTT, and debris was pelleted by centrifugation at 10,000 × g for 20 min at 4°C. 100 μg of total protein were resolved by PAGE, and XDH activity was assayed in gel as described (Lee et al., 2002). Signal intensity was determined using the NIH Image program (http://rsb.info.nih.gov/nih-image/).

Ferrochelatase

Tissues were homogenized in 50 mM Tris-HCl (pH 7.6) and 20% glycerol, and debris was pelleted by centrifugation at 300 × g for 10 min at 4°C. FECH activity was determined by fluorometric monitoring of Zn-mesoporphyrin synthesis as described (Lyoumi et al., 2007) and was expressed as nanomoles of Zn-mesoporphyrin formed per hour per milligram of protein at 37°C.

ETC and TCA Cycle

Tissues were homogenized in 20 mM Tris-HCl (pH 7.4), 250 mM sucrose, 50 mM KCl, and 5 mM MgCl2, and homogenates were centrifuged at 600 × g for 10 min at 4°C. Steady-state activity of ETC and TCA enzyme complexes in the supernatant was determined as described (Sauer et al., 2005) using a temperature-controlled computer-tunable spectrophotometer (Spectramax Plus Microplate Reader, Molecular Devices, Sunnyvale, CA) operating in the dual wavelength mode. The addition of standard respiratory chain inhibitors was used to ascertain the specificity of the enzymatic assays. All enzymatic activities were calibrated to protein concentration.

(I) Model illustrating the central role of the IRP/IRE system for mitochondrial iron sufficiency and function. Mitochondria convert iron into bioactive forms (i.e., ISC and heme) to sustain their own needs as well as supplying heme and (presumably) ISCs to the rest of the cell. By controlling cellular iron uptake, efflux, and storage, IRPs secure sufficient cytosolic iron availability for mitochondrial import and subsequent utilization by the ISC and heme biosynthetic pathways.
See also Figures S3 and S4.

Determination of Total and Mitochondrial Iron Levels

Total nonheme iron content of the liver was determined as described (Galy et al., 2005b). For the determination of mitochondrial iron levels, fresh liver samples were rinsed, finely minced, and homogenized in 4 ml of buffer A (20 mM Tris-HCl [pH 7.4], 250 mM saccharose, 50 mM KCl, and 5 mM MgCl2) using a Dounce homogenizer. The homogenate was centrifuged at 600 × g for 10 min. The pellet was resuspended in 10 ml of buffer A and centrifuged for 10 min at 3,000 × g three times. The crude mitochondrial pellet was resuspended in 100 μl of buffer A, and protein concentration was determined using the D_C protein assay (BioRad). 10 μl of mitochondrial suspension were mixed with 90 μl of 10% HCl + 10% TCA and incubated overnight at 45°C. The samples were centrifuged for 10 min at 10,000 × g, and the supernatant was incubated for 10 min with five volumes of 7M Na acetate, bathophenanthroline-disulfonic acid 0.01%, and thioglycolic acid 0.1%. The OD was measured at 535 nm. For each sample, the blank absorbance was determined by omitting the bathophenanthroline chromogen. The amount of iron was inferred from the serial dilution of a standard iron solution (iron atomic spectroscopy standard, Fluka, Sigma-Aldrich).

Measurement of Heme and Protoporphyrin Levels

The hepatic heme content was determined as described (Delaby et al., 2008). Liver tissue was homogenized in 1:10 w/v ice-cold 50 mM phosphate buffer (pH 7.5), and debris was pelleted by centrifugation at 10,000 × g for 10 min at 4°C. The supernatant was diluted at a 1:5 ratio with saline and passed through a C18 column (Varian, Les Ulis, France). After three washes with water, heme was eluted with formic acid and heme concentration was determined spectrophotometrically at 400 nm using hemin (Orphan Europe; Paris, France) as a standard. Protoporphyrin was extracted from liver tissue and quantified by HPLC and fluorescence emission scanning using a RF540 spectrofluorimeter (Shimadzu Co) and a protoporphyrin standard (Frontier Scientific, Carnforth, Lancashire, UK) as described (Lyoumi et al., 2008).

Microscopy Analyses

For light microscopy, liver samples were fixed in formaldehyde and embedded in paraffin. Periodic acid Schiff staining images were acquired using the AxioVision 4.7.1 software and a Zeiss Imager D1 microscope equipped with a AxioCam HRc camera (Zeiss, Jena, Germany). For electron microscopy, liver samples were fixed in Karnovsky's solution and embedded in araldite. Ultrathin sections were viewed using a Zeiss 900 electron microscope.

Statistical Analyses

Differences between mean values were evaluated by two-tailed Student's t test using the Prism software (GraphPad Software, La Jolla, CA). A p value < 0.05 was considered significant.

SUPPLEMENTAL INFORMATION

Supplemental Information includes Supplemental Experimental Procedures, four figures, and two tables and can be found with this article online at doi:10.1016/j.cmet.2010.06.007.

ACKNOWLEDGMENTS

We wish to thank H. Puccio and A. Martelli for the PPAT-encoding plasmids and anti-PPAT antibody and for their valuable input; G. Schütz for the albumin/α-fetoprotein-Cre strain; G.F. Hoffmann and J.G. Okun for helpful discussions; C. Peyssonaux for recommendations regarding EPAS1 immunodetection; and the staff of the EMBL LAR for their dedicated animal care. We also thank F. Canonne-Hergaux, R. Eisenstein, and B. Paw for their kind gift of antibodies against DMT1, ACO2, and SLC25A37, respectively. This work was supported, in part, by an EEC FP6 grant (LSHM-CT-2006-037296 Euroiron1) and a grant from the BMBF (HepatoSys) to M.W.H.

Received: December 9, 2009
Revised: April 6, 2010
Accepted: June 2, 2010
Published: August 3, 2010

REFERENCES

Ajioka, R.S., Phillips, J.D., and Kushner, J.P. (2006). Biosynthesis of heme in mammals. Biochim. Biophys. Acta *1763*, 723–736.

Andrews, N.C. (2008). Forging a field: the golden age of iron biology. Blood *112*, 219–230.

Atamna, H., Walter, P.B., and Ames, B.N. (2002). The role of heme and iron-sulfur clusters in mitochondrial biogenesis, maintenance, and decay with age. Arch. Biochem. Biophys. *397*, 345–353.

Chen, O.S., Schalinske, K.L., and Eisenstein, R.S. (1997). Dietary iron intake modulates the activity of iron regulatory proteins and the abundance of ferritin and mitochondrial aconitase in rat liver. J. Nutr. *127*, 238–248.

Dallman, P.R. (1986). Biochemical basis for the manifestations of iron deficiency. Annu. Rev. Nutr. *6*, 13–40.

Dallman, P.R., and Goodman, J.R. (1970). Enlargement of mitochondrial compartment in iron and copper deficiency. Blood *35*, 496–505.

Davies, R., Schuurman, A., Barker, C.R., Clothier, B., Chernova, T., Higginson, F.M., Judah, D.J., Dinsdale, D., Edwards, R.E., Greaves, P., et al. (2005). Hepatic gene expression in protoporphyic Fech mice is associated with cholestatic injury but not a marked depletion of the heme regulatory pool. Am. J. Pathol. *166*, 1041–1053.

Delaby, C., Pilard, N., Puy, H., and Canonne-Hergaux, F. (2008). Sequential regulation of ferroportin expression after erythrophagocytosis in murine macrophages: early mRNA induction by haem, followed by iron-dependent protein expression. Biochem. J. *411*, 123–131.

Galy, B., Ferring, D., and Hentze, M.W. (2005a). Generation of conditional alleles of the murine Iron Regulatory Protein (IRP)-1 and -2 genes. Genesis *43*, 181–188.

Galy, B., Ferring, D., Minana, B., Bell, O., Janser, H.G., Muckenthaler, M., Schümann, K., and Hentze, M.W. (2005b). Altered body iron distribution and microcytosis in mice deficient in iron regulatory protein 2 (IRP2). Blood *106*, 2580–2589.

Galy, B., Ferring-Appel, D., Kaden, S., Gröne, H.J., and Hentze, M.W. (2008). Iron regulatory proteins are essential for intestinal function and control key iron absorption molecules in the duodenum. Cell Metab. *7*, 79–85.

Garcia, E.L., and Mills, A.A. (2002). Getting around lethality with inducible Cre-mediated excision. Semin. Cell Dev. Biol. *13*, 151–158.

Graham, R.M., Chua, A.C., Herbison, C.E., Olynyk, J.K., and Trinder, D. (2007). Liver iron transport. World J. Gastroenterol. *13*, 4725–4736.

Guernsey, D.L., Jiang, H., Campagna, D.R., Evans, S.C., Ferguson, M., Kellogg, M.D., Lachance, M., Matsuoka, M., Nightingale, M., Rideout, A., et al. (2009). Mutations in mitochondrial carrier family gene SLC25A38 cause nonsyndromic autosomal recessive congenital sideroblastic anemia. Nat. Genet. *41*, 651–653.

Huang, M.L., Becker, E.M., Whitnall, M., Rahmanto, Y.S., Ponka, P., and Richardson, D.R. (2009). Elucidation of the mechanism of mitochondrial iron loading in Friedreich's ataxia by analysis of a mouse mutant. Proc. Natl. Acad. Sci. USA *106*, 16381–16386.

Kellendonk, C., Opherk, C., Anlag, K., Schütz, G., and Tronche, F. (2000). Hepatocyte-specific expression of Cre recombinase. Genesis *26*, 151–153.

LaVaute, T., Smith, S., Cooperman, S., Iwai, K., Land, W., Meyron-Holtz, E., Drake, S.K., Miller, G., Abu-Asab, M., Tsokos, M., et al. (2001). Targeted deletion of the gene encoding iron regulatory protein-2 causes misregulation of iron metabolism and neurodegenerative disease in mice. Nat. Genet. *27*, 209–214.

Lee, H.J., Adham, I.M., Schwarz, G., Kneussel, M., Sass, J.O., Engel, W., and Reiss, J. (2002). Molybdenum cofactor-deficient mice resemble the phenotype of human patients. Hum. Mol. Genet. *11*, 3309–3317.

Levi, S., and Rovida, E. (2009). The role of iron in mitochondrial function. Biochim. Biophys. Acta *1790*, 629–636.

Liuzzi, J.P., Aydemir, F., Nam, H., Knutson, M.D., and Cousins, R.J. (2006). Zip14 (Slc39a14) mediates non-transferrin-bound iron uptake into cells. Proc. Natl. Acad. Sci. USA *103*, 13612–13617.

Lyoumi, S., Abitbol, M., Andrieu, V., Henin, D., Robert, E., Schmitt, C., Gouya, L., de Verneuil, H., Deybach, J.C., Montagutelli, X., et al. (2007). Increased plasma transferrin, altered body iron distribution, and microcytic hypochromic anemia in ferrochelatase-deficient mice. Blood *109*, 811–818.

Lyoumi, S., Martin-Schmitt, C., Touitou, Y., Puy, H., and Djeridane, Y. (2008). Melatonin and environmental lighting regulate ALA-S gene expression and So porphyrin biosynthesis in the rat harderian gland. Chronobiol. Int. *25*, 851–867.

Mantena, S.K., King, A.L., Andringa, K.K., Eccleston, H.B., and Bailey, S.M. (2008). Mitochondrial dysfunction and oxidative stress in the pathogenesis of alcohol- and obesity-induced fatty liver diseases. Free Radic. Biol. Med. *44*, 1259–1272.

Masini, A., Salvioli, G., Cremonesi, P., Botti, B., Gallesi, D., and Ceccarelli, D. (1994). Dietary iron deficiency in the rat. I. Abnormalities in energy metabolism of the hepatic tissue. Biochim. Biophys. Acta *1188*, 46–52.

Meyron-Holtz, E.G., Ghosh, M.C., Iwai, K., LaVaute, T., Brazzolotto, X., Berger, U.V., Land, W., Ollivierre-Wilson, H., Grinberg, A., Love, P., and Rouault, T.A. (2004). Genetic ablations of iron regulatory proteins 1 and 2 reveal why iron regulatory protein 2 dominates iron homeostasis. EMBO J. *23*, 386–395.

Muckenthaler, M.U., Galy, B., and Hentze, M.W. (2008). Systemic iron homeostasis and the iron-responsive element/iron-regulatory protein (IRE/IRP) regulatory network. Annu. Rev. Nutr. *28*, 197–213.

Nemeth, E., and Ganz, T. (2006). Regulation of iron metabolism by hepcidin. Annu. Rev. Nutr. *26*, 323–342.

Paradkar, P.N., Zumbrennen, K.B., Paw, B.H., Ward, D.M., and Kaplan, J. (2009). Regulation of mitochondrial iron import through differential turnover of mitoferrin 1 and mitoferrin 2. Mol. Cell. Biol. *29*, 1007–1016.

Puy, H., Gouya, L., and Deybach, J.C. (2010). Porphyrias. Lancet *375*, 924–937.

Rouault, T.A., and Tong, W.H. (2008). Iron-sulfur cluster biogenesis and human disease. Trends Genet. *24*, 398–407.

Sauer, S.W., Okun, J.G., Schwab, M.A., Crnic, L.R., Hoffmann, G.F., Goodman, S.I., Koeller, D.M., and Kölker, S. (2005). Bioenergetics in glutaryl-coenzyme A dehydrogenase deficiency: a role for glutaryl-coenzyme A. J. Biol. Chem. *280*, 21830–21836.

Schmidt-Supprian, M., and Rajewsky, K. (2007). Vagaries of conditional gene targeting. Nat. Immunol. *8*, 665–668.

Shaw, G.C., Cope, J.J., Li, L., Corson, K., Hersey, C., Ackermann, G.E., Gwynn, B., Lambert, A.J., Wingert, R.A., Traver, D., et al. (2006). Mitoferrin is essential for erythroid iron assimilation. Nature *440*, 96–100.

Sheftel, A.D., and Lill, R. (2009). The power plant of the cell is also a smithy: the emerging role of mitochondria in cellular iron homeostasis. Ann. Med. *41*, 82–99.

Smith, S.R., Ghosh, M.C., Ollivierre-Wilson, H., Hang Tong, W., and Rouault, T.A. (2006). Complete loss of iron regulatory proteins 1 and 2 prevents viability of murine zygotes beyond the blastocyst stage of embryonic development. Blood Cells Mol. Dis. *36*, 283–287.

Swick, R.A., Cheeke, P.R., and Buhler, D.R. (1982). Subcellular distribution of hepatic copper, zinc and iron and serum ceruloplasmin in rats intoxicated by oral pyrrolizidine (Senecio) alkaloids. J. Anim. Sci. *55*, 1425–1430.

Tong, W.H., and Rouault, T.A. (2006). Functions of mitochondrial ISCU and cytosolic ISCU in mammalian iron-sulfur cluster biogenesis and iron homeostasis. Cell Metab. *3*, 199–210.

Wallander, M.L., Leibold, E.A., and Eisenstein, R.S. (2006). Molecular control of vertebrate iron homeostasis by iron regulatory proteins. Biochim. Biophys. Acta *1763*, 668–689.

Yang, X., Zhang, Y.K., Esterly, N., Klaassen, C.D., and Wan, Y.J. (2009). Gender disparity of hepatic lipid homoeostasis regulated by the circadian clock. J. Biochem. *145*, 609–623.